Volume 4 | Number 3 | 21 January 2016 | Pages 351–558

# Journal of Materials Chemistry B

Materials for biology and medicine

www.rsc.org/MaterialsB

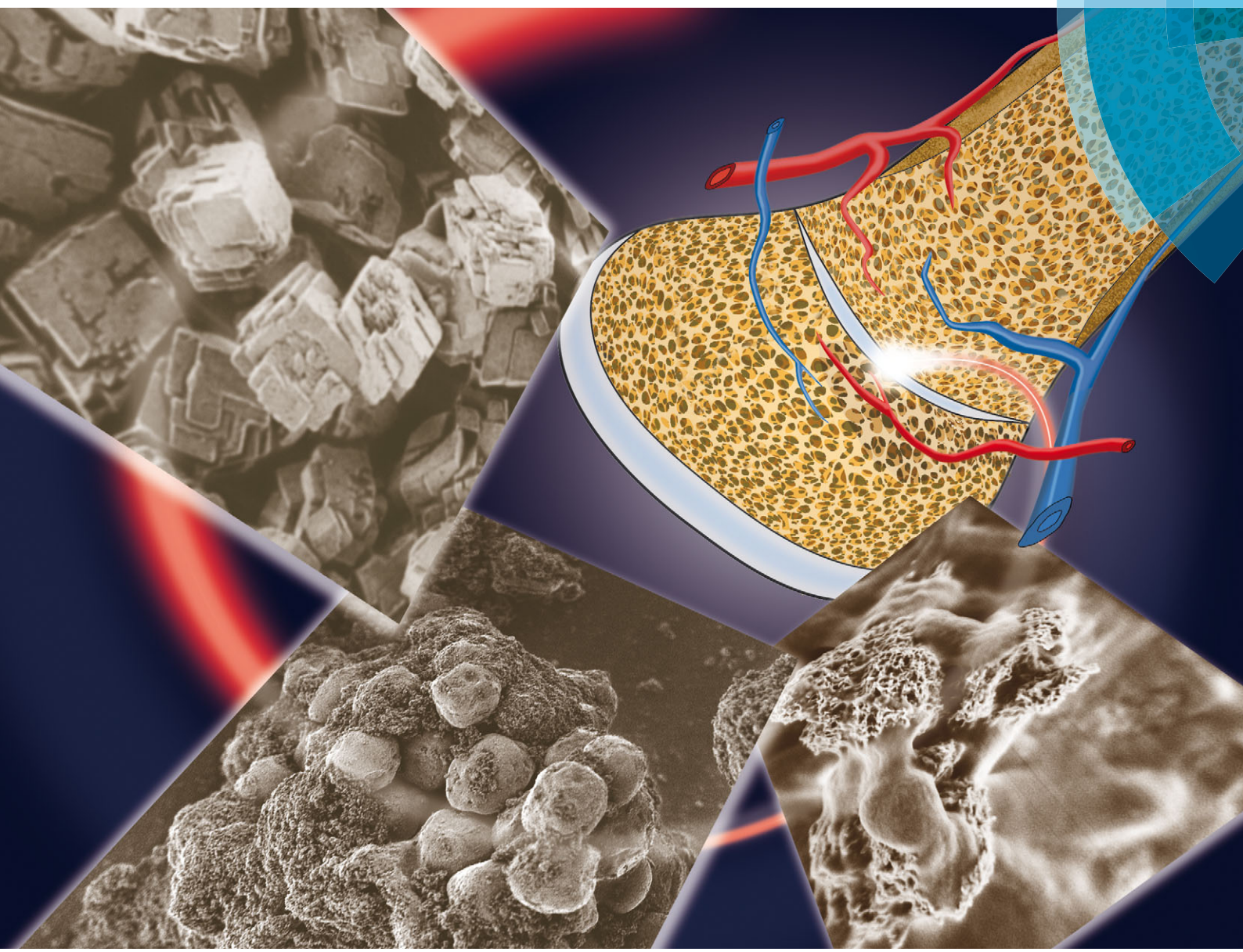

ISSN 2050-750X

ROYAL SOCIETY OF CHEMISTRY

PAPER

Werner E. G. Müller, Xiaohong Wang *et al.*

High biocompatibility and improved osteogenic potential of amorphous calcium carbonate/vaterite

175 YEARS

Journal of
Materials Chemistry B

PAPER

View Article Online
View Journal | View Issue



Cite this: *J. Mater. Chem. B*, 2016, 4, 376

# High biocompatibility and improved osteogenic potential of amorphous calcium carbonate/vaterite

Emad Tolba,[a] Werner E. G. Müller,*[a] Bothaina M. Abd El-Hady,[b] Meik Neufurth,[a] Frederik Wurm,[c] Shunfeng Wang,[a] Heinz C. Schröder[a] and Xiaohong Wang*[a]

Received 25th October 2015,
Accepted 20th November 2015

DOI: 10.1039/c5tb02228b

www.rsc.org/MaterialsB

In human bone, amorphous calcium carbonate (ACC) is formed as a precursor of the crystalline carbonated apatite/hydroxyapatite (HA). Here we describe that the metastable ACC phase can be stabilized by inorganic polyphosphate (polyP) that is also used as a phosphate source for the non-enzymatic carbonate/phosphate exchange during HA formation. This polymer was found to suppress the transformation of ACC into crystalline $CaCO_3$ at a percentage of 5% [w/w] (''CCP5'') with respect to $CaCO_3$ and almost completely at 10% [w/w] (''CCP10''). Both preparations ($CaCO_3$/polyP) are amorphous, but also contain small amounts of vaterite, as revealed by XRD, FTIR and SEM analyses. They did not affect the growth/viability of SaOS-2 cells. Cell culture and $Ca^{2+}$ release experiments revealed that the $CaCO_3$ particles formed in the presence of polyP ($CaCO_3$/polyP) are degradable and, unlike calcite, become disintegrated with time during the cell culture incubation. Again in contrast to calcite, ''CCP5'' and *''CCP10''* were found to exhibit osteogenic activity and induce the expression of *alkaline phosphatase* gene in SaOS-2 cells as well as in human mesenchymal stem cells (MSC). *In vivo* studies in rats, using PLGA microspheres inserted in the muscles of the back of the animals, revealed that the encapsulated ''CCP10'' is not only biocompatible but also supports the regeneration at the implant region. We conclude that ACC containing small amounts of vaterite has osteogenic potential and offers superior properties compared to the biologically inert calcite with respect to a potential application as a scaffold material for bone implants.

## 1. Introduction

Calcium carbonate ($CaCO_3$), the world largest geochemical reservoir for carbon,[1] exists in three major crystalline polymorphs, as calcite, aragonite, and vaterite (reviewed in ref. 2). The amorphous calcium carbonate (ACC) is the least stable polymorph of $CaCO_3$ and vaterite the thermodynamically least stable form of crystalline $CaCO_3$. While calcite and aragonite are common in biological and geological samples, vaterite is metastable and rare in nature (reviewed in ref. 3). Vaterite is occasionally found in biological materials, *e.g.* as a skeletal element in the mussel *Hyriopsis cumingii* and in otoliths (reviewed in ref. 4 and 5). It is remarkable that in fish two of the three pairs of otoliths, the sagittae and the lapilli are composed of aragonite, while the asteriscus are made of vaterite.[6] Biochemical/chemical studies revealed that the mature crystals of otoliths are metabolically inert crystalline skeletal structures which run in parallel with organic matrices that vary. This observation suggested that those organics might act as templates as well as structure-guiding molecules during the deposition of the mineral phase from the amorphous to the distinct mineral phase.[3] The importance of the organic components as a structure and function orientating guide within the skeletal inorganic deposits has been postulated and finally proven in several biological systems, *e.g.* in shell layers of some mollusks[7] or in calcareous spicules from sponges.[8] The crucial role of acidic matrix macromolecules, intimately involved in the growth of biological crystals, has been highlighted already in 1985[9] and later corroborated multifold, *e.g.* in the hic31 framework-matrix protein within the prismatic-layer of *H. cumingii*.[10]

The basic building blocks of bone comprise, besides water and collagen, a form of carbonated apatite similar to dahllite [$Ca_5(PO_4,CO_3)_3(OH)$] (reviewed in ref. 11 and 12). This crystalline mineral is likely to be formed from amorphous calcium

[a] *ERC Advanced Investigator Grant Research Group at the Institute for Physiological Chemistry, University Medical Center of the Johannes Gutenberg University, Duesbergweg 6, D-55128 Mainz, Germany. E-mail: wmueller@uni-mainz.de, wang013@uni-mainz.de; Fax: +49 6131-39-25243; Tel: +49 6131-39-25910*
[b] *Biomaterials Department, Inorganic Chemical Industries Division, National Research Center, Doki 11884, Cairo, Egypt*
[c] *Department of Physical Chemistry of Polymers, Max Planck Institute for Polymer Research, Ackermannweg 10, D-55128 Mainz, Germany*

phosphate (ACP).[13] Very recently biochemical and dispersive spectroscopic evidence suggested that it is ACC that acts as a bioseed for the formation of carbonated apatite,[14] a process that is accelerated by carbonic anhydrase(s) (CA), very likely by the soluble CA-II isoform[14] and/or the cell-membrane-associated CA-IX.[15–17] Based on the evidence the following three mechanically distinct phases resulting in bone hydroxyapatite (HA) formation can be distinguished;[18] first, enzymatic formation of ACC bioseeds *via* CAes, second, non-enzymatic exchange of carbonate ions by phosphate[19] in the formation of ACP and third, transition of ACP to the crystalline phase carbonated apatite/HA. It should be mentioned that polyphosphate (polyP), which is present in considerable amounts in the blood and in larger extent in blood platelets, has been implicated as a phosphate source for the formation of the bone calcium phosphate deposits (reviewed in ref. 18). From this polymer *ortho*-phosphate is enzymatically removed *via* the alkaline phosphatase (ALP)[20] which might serve as a donor for bone mineralization. In addition, octacalcium phosphate and osteopontin, phosphorylated bone matrix glycoproteins, have been discussed as precursors of biological apatite crystal formation.[21]

In recent years, bioinspired as well as biomimetic approaches have been undertaken to develop functional materials capable of promoting bone tissue regeneration. Since collagen and HA are dominant in bone, biomaterials containing chemical-inducers of any of these materials or both have been extensively explored in bone tissue engineering with the hope to accelerate bone regeneration (reviewed in ref. 22). Calcium phosphate salts in general and HA in particular have been found to be superior as regenerative materials than their non-mineralized counterparts (reviewed in ref. 23). The application of ACC as a potential regeneration-inducing/supporting material has been hampered by the fact that ACC, as such, is not stable. Stabilization of ACC *in vivo* is regulated by specialized proteins, often in combination with $Mg^{2+}$, while under *in vitro* conditions non-biogenic additives, like soluble polycarboxylates, again $Mg^{2+}$, triphosphate, or polyphosphonate species freeze ACC to a relative stable phase (see ref. 24 and 25); also freeze-drying has been determined to stabilize ACC.[26] In contrast, vaterite is stable enough to allow dissociation and in turn might act as a potential ion buffering system for bone regeneration and by that could modify transformation processes from $CaCO_3$ to HA.[27]

In the present study we describe that polyP can stabilize the ACC phase. Previously it has been reported that soluble Na-polyP, spiked with defined molar ratios of $Ca^{2+}$, can be processed to solid nanoscaled nano-/microparticles that remain amorphous.[28,29] In contrast, other polyP based ceramics have been prepared as crystalline materials at high temperature[30,31] or as a phosphate glass of variable chemical and physical structures as well as particle morphologies in the microsize range.[32] In our procedure, at a level of 5% [w/w], polyP considerably suppresses the transformation of ACC to crystalline $CaCO_3$ and at a percentage of 10% [w/w] the polymer almost completely blocks this process. This finding might have important implications since polyP is a natural polymer which is abundantly present in the circulated blood and also in blood platelets.[33,34] Previously, polyP has been found to act as a morphogenetically active inorganic molecule on bone cells and induces their mineralization potency. The present study shows that $CaCO_3$, containing 5 or 10% [w/w] of polyP, comprises osteogenic potential in SaOS-2 cells as well as in human mesenchymal stem cells (MSC) by inducing *ALP* gene expression. In addition, it is shown that this calcium carbonate/calcium phosphate hybrid material is biocompatible and supports regeneration *in vivo*.

## 2. Material and methods

### 2.1 Materials

Na-polyphosphate (Na-polyP) with an average chain length of $\approx$40 phosphate units was obtained from Chemische Fabrik Budenheim (Budenheim, Germany). Poly(D,L-lactide-*co*-glycolide) (PLGA; lactide : glycolide [75 : 25]; mol wt 66 000–107 000; P1941) was obtained from Sigma (Taufkirchen, Germany).

### 2.2 Preparation of Ca-carbonate microparticles

Ca-carbonate ($CaCO_3$) was prepared by direct precipitation in aqueous solutions (at room temperature), using $CaCl_2{\cdot}2H_2O$ solution (#223506; Sigma-Aldrich, Taufkirchen, Germany) and $Na_2CO_3$ solution (#85195; Fluka-Sigma) at an equimolar concentration ratio between $Ca^{2+}$ and $CO_3^{2-}$ through rapid mixing. In brief, 20 mL of 0.1 M NaOH was added to 1.05 g $Na_2CO_3$ and then diluted with 30 mL of deionized water. This solution was combined with 50 mL of water containing 1.47 g $CaCl_2{\cdot}2H_2O$ and then rapidly stirred, immediately followed by filtration. The $CaCO_3$ precipitate (termed "CC") was rinsed with acetone to dry the solid material; scheme in Fig. 1.

To study the effect of polyP on precipitated $CaCO_3$ the solution of 20 mL of 0.1 M NaOH was supplemented with 0.05 g or 0.1 g of Na-polyP to which 1.05 g of $Na_2CO_3$ was added; subsequently this solution was diluted with 30 mL of deionized water. Then 50 mL water, containing 1.47 g $CaCl_2{\cdot}2H_2O$, was added. After this, 5% [w/w] (addition of 0.05 g Na-polyP) and 10% [w/w] (0.1 g Na-polyP) of polyP, respectively, was added to the $CaCO_3$ precipitation assay. The suspensions obtained were filtrated, washed with acetone and dried at room temperature. The samples were termed "CCP5" (0.05 g Na-polyP per $CaCO_3$ precipitation assay) or "CCP10" (0.1 g).

### 2.3 X-ray diffraction analyses

X-ray diffraction (XRD) experiments were performed as described previously.[35] The patterns of dried powders were registered on a Philips PW 1820 diffractometer with CuK$\alpha$ radiation ($\lambda$ = 1.5418 Å, 40 kV, 30 mA) in the range $2\theta$ = 5–65° ($\Delta 2\theta$ = 0.02, $\Delta t$ = 5 s). The calcite and vaterite phases were identified as described.[36,37]

### 2.4 Fourier transformed infrared spectroscopy

Fourier transformed infrared spectroscopic (FTIR) analyses were performed with micro-milled (agate mortar and pestle) mineral powder in an ATR (attenuated total reflectance)-FTIR spectroscope/Varian 660-IR spectrometer (Agilent, Santa Clara, CA),

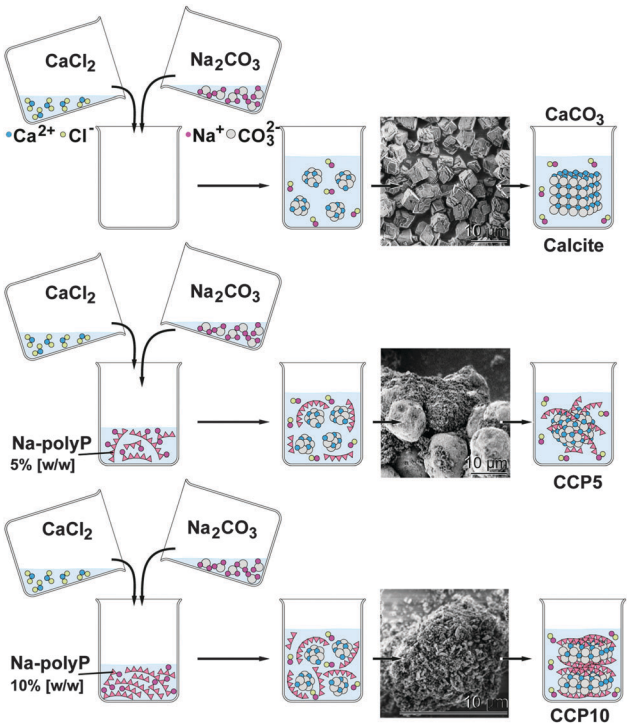


Fig. 1 Preparation of calcite and $CaCO_3$ supplemented with polyP (scheme). The insets show the SEM images of the respective product.

fitted with a Golden Gate ATR unit (Specac, Orpington, UK).[19] The spectra given represent the average of 100 scans with a spectral resolution of 4 $cm^{-1}$ (typically 550–4000 $cm^{-1}$). The baseline correction, smoothing, and analysis of the spectra were achieved using the Varian 660-IR software package 5.2.0 (Agilent). Graphical display and annotation of the spectra were performed with Origin Pro (version 8.5.1; OriginLab, Northampton, MA).

### 2.5 Scanning electron microscopic studies

Scanning electron microscopic (SEM) analyses were performed using an SU 8000 instrument (Hitachi High-Technologies Europe, Krefeld, Germany), at low voltage (1 kV) as described.[38] The particle size was determined using a particle size analyzer (ImageJ); 25–50 crystals were evaluated.

### 2.6 Release of $Ca^{2+}$ from $CaCO_3$ particles

In separate assays 100 μg $mL^{-1}$ of either calcite or "CCP10" were added into an Eppendorf tube containing 1 mL of 1 M Tris-HCl (pH 7.4). After incubating at room temperature for 2 h, 2 d, 3 d and 8 d samples of 100 μL were taken, centrifuged and the supernatant analyzed for $Ca^{2+}$ concentration. The determination was performed using a the photometric test kit (Millipore/Merck Chemicals, Darmstadt, Germany; article no. 100858 "Calcium Cell Test") as per manufacturer's instructions. The blank values were subtracted from the test assays.

### 2.7 Cultivation of SaOS-2 cells

The human osteogenic sarcoma cells SaOS-2 (#89050205; Sigma) were cultured in McCoy's medium (Biochrom-Seromed, Berlin, Germany), supplemented with 2 mM L-glutamine and enriched with 15% heat-inactivated fetal calf serum (FCS).[39] Antibiotics, 100 units per mL penicillin and 100 μg $mL^{-1}$ streptomycin, were likewise added. The cells were incubated in 25 $cm^2$ flasks or in 6-well plates (growth area 9.5 $cm^2$; Corning Costar cell culture plates; #CLS3516 Sigma) at 37 °C. The cultures were inoculated with $1 \times 10^4$ cells per well in a total volume of 3 mL. Where indicated, the cultures were first incubated for a period of 3 d in the absence of the mineralization-activating cocktail (MAC). Then the cultures were continued to be incubated for additional 7 d in the absence or presence of the MAC, comprising 5 mM β-glycerophosphate, 50 mM ascorbic acid and 10 nM dexamethasone to induce biomineralization.[40] The $CaCO_3$ samples ("CC", "CCP5" or "CCP10") were added to each well at the beginning of the experiments. Every third day the culture medium was replaced by fresh medium/serum and, where indicated, also with MAC. The cells were subsequently used for the quantification of the *ALP* gene expression.

### 2.8 Cell viability assay

SaOS-2 cells were seeded into the 6-well plates and cultured for 3 d in McCoy's medium/15% FCS. Where indicated, the cultures were supplemented with 30 μg (in 3 mL) of the respective $CaCO_3$ preparation. Then, after a 2 or 3 d incubation period, the cells were incubated with fresh medium containing 200 μL of 3-[4,5-dimethyl thiazole-2-yl]-2,5-diphenyl tetrazolium (MTT; #M2128, Sigma) for 4 h in the dark. Subsequently the remaining MTT dye was aspirated and 200 μL of DMSO were added to solubilize the formazan crystals. Finally, the optical densities (OD) were determined at 650 nm.[14] Ten parallel experiments each were performed.

### 2.9 Human mesenchymal stem cells

The expression of *ALP* was determined, in parallel in SaOS-2 cells, and also in human mesenchymal stem cells (MSC). The cells were isolated using previously described methods; the experiments had been approved by the ethics committee.[41,42] The deep-frozen, preserved MSCs were thawed, and suspended in 75 $cm^2$ flasks. They were cultivated in α-MEM (Cat. no. F0915; Biochrom, Berlin, Germany), supplemented with 20% FCS supplemented with 0.5 mg $mL^{-1}$ of gentamycin, 100 units penicillin, 100 μg $mL^{-1}$ of streptomycin and 1 mM pyruvate (#P2256 Sigma-Aldrich). The incubation was performed in a humidified incubator at 37 °C. After the pre-incubation period of 3 d the non-adherent cells were discarded, and the adherent cells were continued to be incubated with α-MEM/FCS.

### 2.10 Quantitative real-time polymerase chain reaction: ALP expression

The SaOS-2 or MSCs cells were pre-cultivated for 3 d in medium/serum. Then the cultures were split and incubated either in the absence of any $CaCO_3$ (control) or with 50 μg $mL^{-1}$ of "CCP5", "CCP10" or calcite and the cultivation was continued for an additional 7 d in the absence or presence of MAC. Subsequently, the cells were harvested, RNA extracted and subjected for quantitative real-time RT [reverse transcription]-polymerase

 

chain reaction (qRT-PCR) as described.[43] The following primer pairs were used: ALP [alkaline phosphatase; NM_000478.4] fwd: 5′-TGCAGTACGAGCTGAACAGGAACA-3′ [$nt_{1141}$ to $nt_{1164}$] and rev: 5′-TCCACCAAATGTGAAGACGTGGGA-3′ [$nt_{1418}$ to $nt_{1395}$; product size of 278 bp] and as reference GAPDH [glyceraldehyde 3-phosphate dehydrogenase; NM_002046.3] fwd: 5′-CCGTCTAGA AAAACCTGCC-3′ [$nt_{929}$ to $nt_{947}$] and rev: 5′-GCCAAATTCGTTGTC ATACC-3′ [$nt_{1145}$ to $nt_{1126}$; 199 bp]. The qRT-PCR determinations were performed in an iCycler (Bio-Rad, Hercules, CA, USA), and the mean $C_t$ values and efficiencies were calculated by iCycler software (Bio-Rad); the estimated PCR efficiencies were in the range of 93%–103%.[39]

### 2.11 Preparation of PLGA-based implant microspheres

The microspheres, used for the animal experiments were produced as described in detail.[44] The implant microspheres lacking $CaCO_3$/polyP were fabricated with 4 mL of a PLGA/dichloromethane solution (volume ratio 1 : 5); they are termed "cont-mic". For the fabrication of the implant spheres containing $CaCO_3$/polyP, "CCP10" was added to the PLGA/dichloromethane mixture at a concentration of 20%. The viscous reaction mixture was pressed through a syringe with an aperture of 0.8 mm. By this approach, implant microspheres, termed "polyP-mic", with an average diameter of ≈830 were obtained (see under "Results").

The content of polyP in the microspheres was proven after treatment of the samples with 1 M sulfuric acid to hydrolyze polyP; the resulting orthophosphate was determined with ammonium molybdate (#277908; Sigma-Aldrich) as described.[45]

### 2.12 Determination of the mechanical properties

The mechanical properties of the microspheres were determined using a nanoindenter, equipped with a cantilever that has been fused to the top of a ferruled optical fiber.[44,46] Using this technique the reduced Young's modulus (RedYM) was determined.

### 2.13 Compatibility studies *in vivo*

Wistar rats of male gender, weighting between 240 g and 290 g (age: two months), were included in this study; 3 animals from each group were used. The animal experiments were performed in compliance with the relevant laws and institutional guidelines; they had been approved by the ethics committee at the Dongzhimen Hospital at the Beijing University of Chinese Medicine (No. 5 Haiyuncang Road, Dongcheng District, Beijing 100700; Beijing Committee of Science and Technology). The certificate number for the approval is 2012-0001; the experimental studies had been performed by Dr Xing YU. Diet and water were provided *ad libitum* during the total experimental period. Prior to surgery the animals were treated with Ciprofloxacins (Bayer, Leverkusen, Germany) 10 mL $kg^{-1}$ of body weight for antibiotic prophylaxis. Then the animals were narcotized with chlorpromazine (Smith, Kline & French, Philadelphia, PA)/Ketamin (Ketanest; Pfizer, Groton, CT) *via* intramuscular injection. Following routine disinfection, incisions of ≈1 cm were made in the right and left half, perpendicularly to the vertebral axis at the upper limb level. Following skin incision, the muscle was incised and dissected to accommodate the microspheres. The implant microspheres (≈20 mg in a volume of 100 μL) were introduced into the muscle and stabilized there in the deeper layer.[44,47,48] After a period of 2, 4, or 8 weeks the animals were sacrificed and the specimens with the surrounding tissue were dissected and sliced. The samples were inspected macroscopically for inflammation, infection and discoloration.

The samples were fixed in formalin, sliced, stained with Mayer's hematoxylin (#MHS1; Sigma) and then analyzed by optical microscopy (using an Olympus AHBT3 microscope).[49]

### 2.14 Statistical analysis

After finding that the values follow a standard normal Gaussian distribution, the results were statistically evaluated using the paired Student's *t*-test.[50]

## 3. Results

### 3.1 Effects of polyP on calcite formation: FTIR and XRD spectra

For all $CaCO_3$ solids the following FTIR signals were recorded: $\nu_1$ (symmetric stretching) at ≈1080 $cm^{-1}$; $\nu_2$ (out of-plane bending) at ≈870 $cm^{-1}$; $\nu_3$ (doubly degenerate planar asymmetric stretching) at ≈1400 $cm^{-1}$ and $\nu_4$ (doubly degenerate planar bending) at 700 $cm^{-1}$. The published IR data,[36] which were obtained with FTIR/KBr pellets, include peaks located at around 1400 $cm^{-1}$ ($\nu_3$), 876 $cm^{-1}$ ($\nu_2$), and 714 $cm^{-1}$ ($\nu_4$) for calcite and 1090 $cm^{-1}$ ($\nu_1$), 870 $cm^{-1}$ ($\nu_2$), and 745 $cm^{-1}$ ($\nu_4$) for vaterite (Fig. 2). Our samples prepared in the absence of polyP are characterized as follows. For calcite the typical vibration bands 1391, 872 and 712 $cm^{-1}$ were recorded, while the samples prepared in the presence of polyP showed the adsorption peaks at 1398, 869 and 742 $cm^{-1}$ for "CCP5" polyP as well as the bands at 1398, 869 and 741 $cm^{-1}$ for "CCP10" proving the formation of vaterite. It is apparent that the strength of the signal for vaterite at around 741 $cm^{-1}$ decreases at a higher content of polyP in the fabricated $CaCO_3$ solids, "CCP10" *versus* "CCP5". This is indicative for the formation of ACC. Besides the $CO_3^{2-}$ absorption peaks, the peaks from 1200 $cm^{-1}$ to 950 $cm^{-1}$ correspond to the absorption peaks of phosphate in polyP.

The above result, vaterite to be formed in small portions in ACC solids, was confirmed with XRD in which the diffraction peaks of the sample prepared in the absence of polyP, at approximately 23°, 30°, 36° and 40°, is given; those signals correspond to calcite. In contrast, the samples prepared in the presence of polyP ("CCP5") showed peaks at approximately 24°, 27°, 32° and 44°, which also reflect the existence of vaterite. Furthermore, these data prove that the $CaCO_3$ solids, prepared in the absence of polyP were pure calcite (Fig. 3A). In contrast, the "CCP5" samples were composed of vaterite in association with ACC, as can be deduced from the low intensities of the signals and also the broadening of the diffraction peaks for sample "CCP5" (Fig. 3B). In consequence, the increase of the amount of polyP, as in "CCP10", causes a decrease transformation rate of ACC to vaterite. This is evident from the XRD pattern of "CCP10" sample which exhibits the amorphous nature of the sample, but also containing small amounts of vaterite.

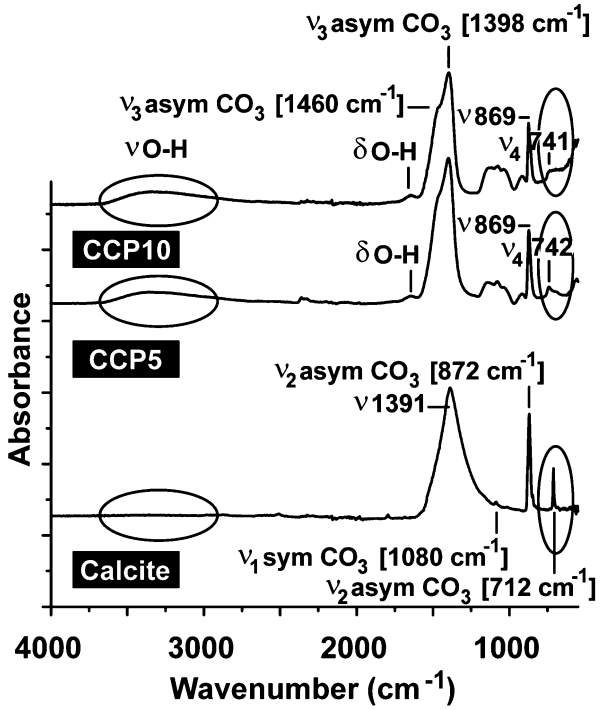


Fig. 2 FTIR spectra of calcite as well as "CCP5" (0.05 g of Na-polyP/assay) and "CCP10" (0.1 g of Na-polyP). The major distinguishing vibration regions/signals for calcite *versus* ACC, the vibration range for O–H (around 3250 $cm^{-1}$) and the asymmetric $\nu_2$ line for $CO_3$ at 712/742 $cm^{-1}$ are circled.

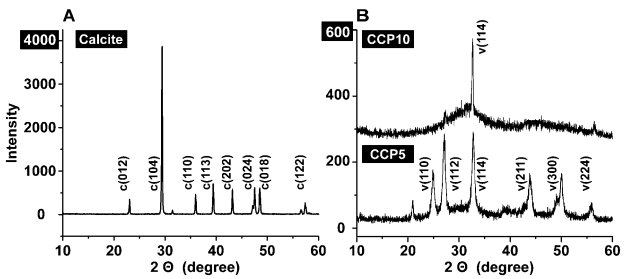


Fig. 3 XRD pattern obtained from (A) calcite and (B) the two $CaCO_3$ preparations, containing two different concentrations of polyP, "CCP5" or "CCP10". The characteristic signals are highlighted and marked with the respective Miller indices, given in parentheses.[36] Please note the different scale of the ordinate captions between (A) and (B).

### 3.2 Morphology of the solids formed

The solids formed by precipitation from $CaCl_2{\cdot}2H_2O$ and $Na_2CO_3$ were studied by SEM. The photomicrographs of the particles, formed in the absence of polyP, show the typical crystalline calcite, the rhombohedral crystals surrounded by {104} faces;[51] Fig. 3A and B. The size of the particles varies between 5.3 to 8.9 ± 2.4 μm. In contrast, those solids formed from $CaCl_2{\cdot}2H_2O$ and $Na_2CO_3$ in the presence of polyP show a different morphology. At the lower polyP concentration, the "CCP5" particles show a spherical appearance with an average size of the spherical crystals of 9.4 ± 3.7 μm (Fig. 4C and D); we attribute these particles to vaterite. They are surrounded by very abundantly accumulating small nanoparticles with a size range

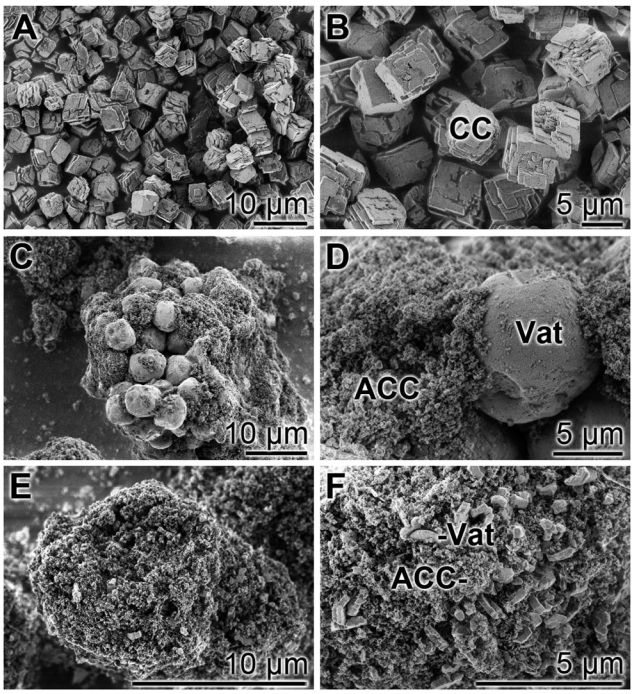


Fig. 4 Morphology of the solids formed from $CaCl_2{\cdot}2H_2O$ and $Na_2CO_3$; SEM analysis. (A and B) In the absence of polyP calcite crystals are formed. This morphology is changed after the addition of polyP during the precipitation process. (C and D) In the presence of 5% polyP, the "CCP5" particles show a spherical appearance. (E and F) At 10% polyP, "CCP10", the solids show a platelet-like shape, which corresponds to vaterite crystals (Vat).

of 100 to 200 nm, which we assigned as ACC. Increasing the polyP, as in "CCP10", the globular particles disappear and are replaced by penta/hexagonal flake shaped vaterite (Fig. 4E and F). High-magnification of the samples by SEM revealed that those individual large flakes, vaterite crystals, are formed by numerous globular to platelet-like, mostly ACC, each about 500 nm. The latter two morphologies, the globular particles and the flake like particles, match the described crystalline vaterite grains.[37]

In turn, the data (XRD, FTIR and SEM) indicate that the "CCP5" and "CCP10" particles consist, to a different proportion, of ACC together with vaterite.

### 3.3 Effects of $CaCO_3$ samples on cell growth/viability

The cell growth/viability of SaOS-2 cells after exposure to the $CaCO_3$ preparations was determined by applying the MTT assay. The $CaCO_3$ samples were added at a concentration of 50 μg $mL^{-1}$ to the cells. In parallel a control series of experiments lacking any $CaCO_3$ solids was performed (Fig. 5). The results revealed that the increase in cell growth/viability from 0.70 ± 0.11 at time 0 to approximately 1.1 absorbance units after 2 d and 2.35 units after 3 days changes only non-significantly among the control assays and the three $CaCO_3$ series ("CCP5", "CCP10" or calcite).

### 3.4 Stability of the $CaCO_3$ solids in the culture medium

SaOS-2 cells grow in an adherent manner.[52] If the cultures are exposed to either calcite or "CCP5" solids the growth behavior onto the surfaces of the culture dishes is similar in assays

 

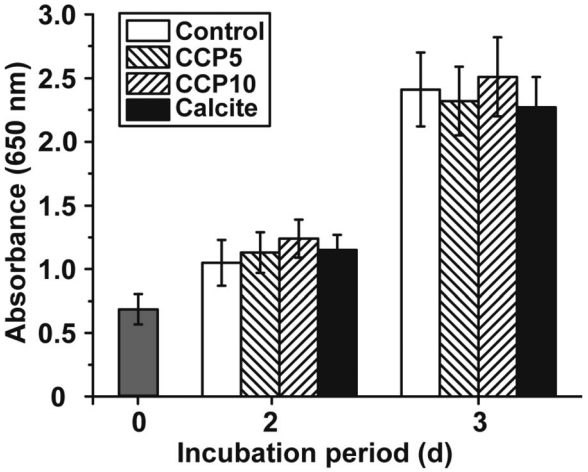


Fig. 5 Cell viability/growth of SaOS-2 cells after cultivation for 2 d and 3 d, respectively, in the absence of any $CaCO_3$ solids (control; open bars) or after exposure to 50 μg $mL^{-1}$ of "CCP5" (left hatched bars), "CCP10" (right hatched bars) or calcite (filled bars). After terminating the cultivation, the assays were subjected to the MTT assay and the absorbance at 650 nm was determined. The absorbance value at time zero is likewise given (grey bars). Data represent means ± SD of ten independent experiments.

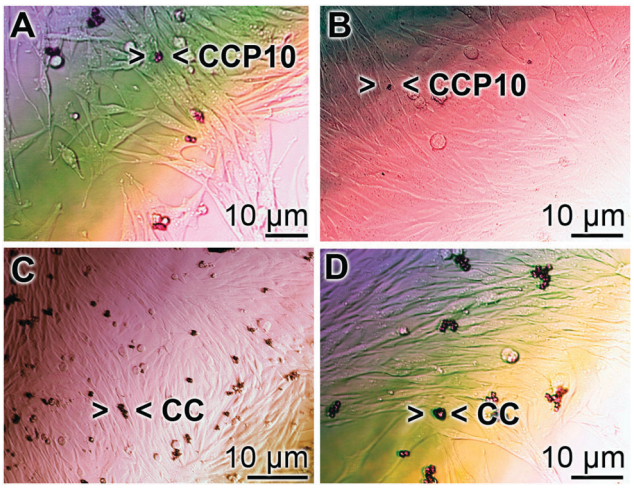


Fig. 6 Growth pattern of SaOS-2 cells in the presence of 50 μg $mL^{-1}$ of "CCP10" (A and B) or calcite (C and D) after a 3 d incubation period. The cells were identified by phase contrast/Nomarski optics. The $CaCO_3$ particles in the assays became visible in the phase contrast images and are marked (><).

containing either "CCP10" (Fig. 6A and B) or calcite (Fig. 6C and D). After 3 d the cells grow almost to confluency. However, it is remarkable that the number of mineral particles, floating in the culture medium, after this period of time, is strongly reduced in the assays containing "CCP10" (Fig. 6A and B), compared to those seen in calcite assays (Fig. 6C and D). This observation can be taken as an indication that the "CCP10" particles undergo dissolution during the 5 d incubation period. This finding is supported by the determination revealing that after 3 d incubation period in simulated body fluids[53] the amount of calcite particles decreases only by 5–10%, while only 35% of the "CCP10" particles can be recovered, as measured on the basis of sedimentable carbonate (data not shown).

### 3.5 Release of $Ca^{2+}$ from $CaCO_3$ particles

In separate assays either calcite or "CCP10" was added into a 1 mL assay, buffered with 1 M Tris-HCl (pH 7.4). While almost no $Ca^{2+}$ is released from the calcite sample, already 6.8 ± 1.1 μg $mL^{-1}$ (68% of the total $Ca^{2+}$ in the reaction mixture) was released from the "CCP10" after a period of 48 h; this extent increases further during the total 192 h of incubation (Fig. 7).

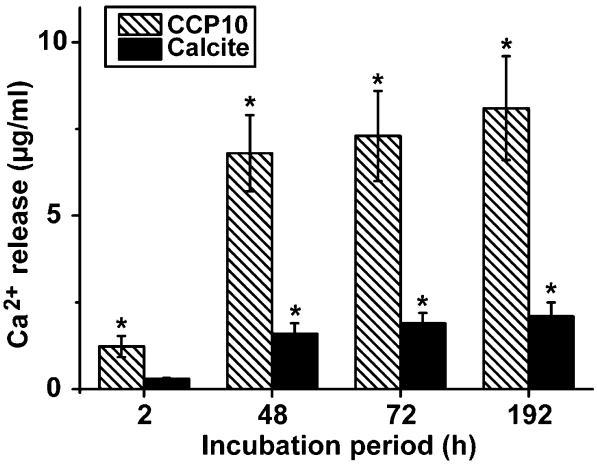


Fig. 7 Release of $Ca^{2+}$ from the $CaCO_3$ particles. "CCP10" or calcite was incubated in Tris-HCl buffer (pH 7.4) for various time periods and the supernatant was analyzed for $Ca^{2+}$ concentration. The results are means from 6 parallel experiments; *$P < 0.01$.

### 3.6 Expression of the ALP in SaOS-2 cells as well as in MSCs

The morphogenetic activity of the $CaCO_3$ samples towards SaOS-2 cells as well as the MSCs was determined in the absence and presence of MAC. Using SaOS-2 cells it was determined that in the absence of MAC the expression ratio between the *ALP* and the reference gene expression (*GAPDH*) significantly increases from 0.31 ± 0.9 arbitrary units to ≈0.6. Within the sets of experiments without the MAC no significant differences are measured, irrespective of the absence (control) or presence of the $CaCO_3$ samples in the assays (Fig. 8A). However, if the expression ratio (*ALP*:*GAPDH*) is determined in MAC activated cells then a significant increase of the ratio to 0.87 ± 0.12 (in the control), to 1.74 ± 0.23 ("CCP5") or to 1.86 ± 0.29 ("CCP10") is measured. In contrast, no response of the cells in assays with calcite is determined (0.14 ± 0.05).

A similar expression pattern of the ALP, if correlated to the reference *GAPDH* gene expression, is found if MSCs are used for the experiments. Again, in the presence of the MAC a significant increase of the expression ratio is seen in assays in the absence of any $CaCO_3$ solid, as well as in the presence of both "CCP5" and "CCP10". No inducing effect is determined in cells exposed to calcite (Fig. 8B).

### 3.7 Implant microspheres, used for the animal studies

The control spheres, the "cont-mic" had a size of (≈845 μm [820 ± 60 μm]; $n$ = 50), while those containing polyP were

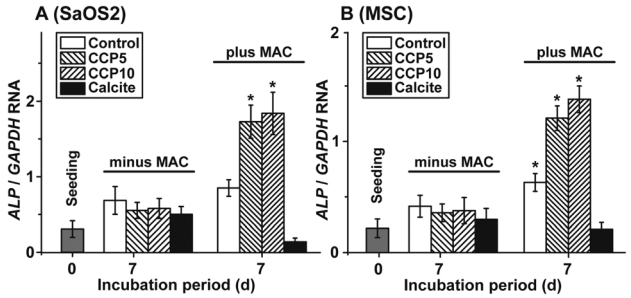


Fig. 8 Steady-state expression levels of the ALP gene both in (A) SaOS-2 cells and in (B) MSCs. The cells remained without any $CaCO_3$ solids (control), or were exposed to 50 μg $mL^{-1}$ of "CCP5" (left hatched bars), "CCP10" (right hatched bars), or calcite (filled bars). After the 3 d pre-incubation period in the absence of MAC the cells were continued to be incubated in the absence of MAC (minus MAC) or were exposed to MAC (plus MAC). After the 7 d incubation the cells were harvested, their RNA extracted and subjected to qRT-PCR analyses. The expression values are given as ratios to the reference gene *GAPDH*; the ratios at time zero are in grey. The results are means from 5 parallel experiments; $*P < 0.01$; the values are computed against the expression measured in cells during seeding.

insignificantly slightly smaller (≈838 μm [816 ± 65 μm]); Fig. 9A and B. The texture of the microsphere surfaces was porous and had pores of 25–30 nm (not shown here). The content of polyP in the "polyP-mic" was 7.26 ± 0.92%. The hardness of the particles (RedYM) was determined using a nanoindenter and found to be for the "cont-mic" 26.99 ± 6.22 MPa and the "polyP-mic" 23.96 ± 5.49 MPa.

### 3.8 Compatibility studies in rats

The implant microsphere samples (20 mg), both "cont-mic" and "polyP-mic", were inserted in the muscles of the back of rats, as described under "Materials and Methods" (Fig. 10A and B). After 2, 4, or 8 week tissue samples with the microspheres were removed, sliced and stained with the hematoxylin solution. In none of the excised specimens any sign for a histopathological alteration could be seen in all of the three sacrificed laboratory animals per group both for the "cont-mic" (Fig. 10C, E and G) and the "polyP-mic" series (Fig. 10D, F and H). Typical images for the sample sections, stained with hematoxylin are shown. It is evident that after 2 weeks the regions, where the implant microspheres had been placed into the muscle, harbor a few cells which are scattered within the implanted microsphere areas (Fig. 10C and D). However, after a 4 (Fig. 10E) and 8 week (Fig. 10G) stay of the "cont-mic" microspheres in the muscle area the implant spheres appear to be empty or close to be cell-free. In contrast, within the "polyP-mic" microspheres already after 4 weeks (Fig. 10F) an accumulation of the cells within the spheres are evident. Even more, after 8 weeks the spheres are almost filled with infiltrating cells (Fig. 10H).

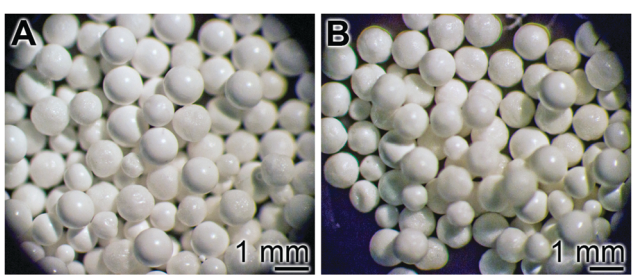


Fig. 9 Morphology of the microspheres; (A) control spheres "cont-mic" and (B) polyP loaded spheres, "polyP-mic".

## 4. Discussion

As any organ in the human body, the skeletal elements are dynamic systems, prone to anabolic and catabolic processes. In contrast *e.g.* to the liver, the inorganic components and especially the crystalline HA part of the bones show a comparably slow metabolic turnover with the relatively low rate of 2 to 3% per year.[54] Basically it can be taken as a rule that crystalline minerals in an organism are biologically inert; typical examples are bladder stones that are formed from crystalline creatinine,

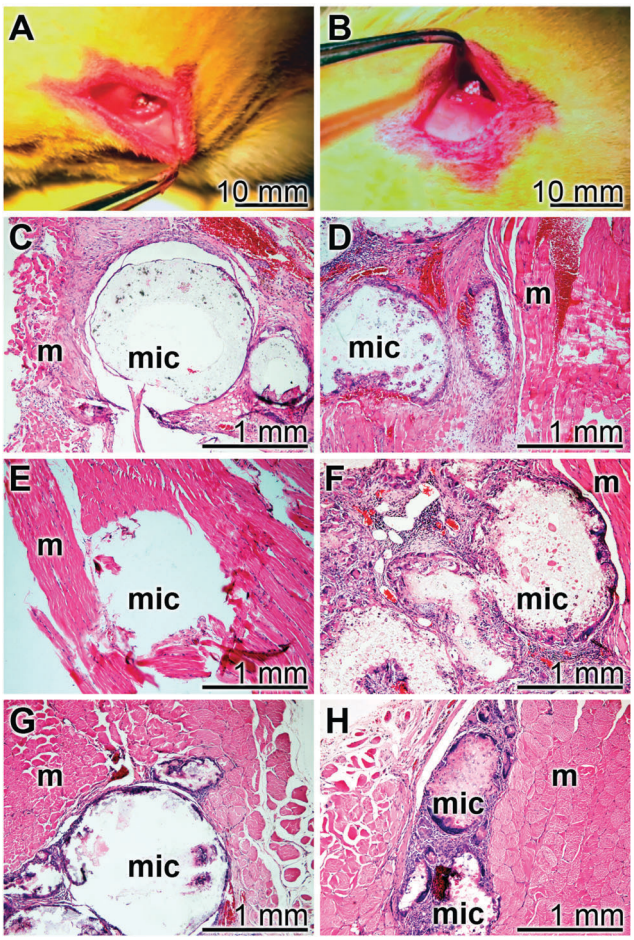


Fig. 10 Implantation of the implant microspheres (A and B) into muscle of the back of a test animal. (C to H) Cytochemical analysis of the regions around the microspheres after a period of 2 weeks (C and D), 4 weeks (E and F) and 8 weeks (G and H) of transplantation. The animals received either "cont-mic" implant microspheres (C, E and G) or implant microspheres ("polyP-mic"), filled with "CCP10"; staining of the slices was performed with hematoxylin. Microspheres (mic) and muscle areas are marked (m).

oxalate, citrate, uric acid, sulfate, chloride and/or ammonium under supersaturated and acidic conditions.[55] In turn, bone implant materials that should elicit regenerative activity might preferentially be formed of amorphous materials, like *e.g.* bioactive glass.[56] Amorphous precursors from HA, *e.g.* ACC or ACP,[57] are metastable phases which give rise to the mature carbonated and subsequently crystalline HA apatite (reviewed in ref. 12). Under physiological conditions, the turnover of HA is, if at all, very low, while the transition from ACC to calcium phosphate runs readily and is only dependent on the substrate/product concentrations.[19] In any event, concentration-dependent reactions in the body are driven enzymatically, since both the process of oversaturation, a result of active metabolic pumping, and the throughput *via* the flow equilibrium are energetically coupled to exergonic reactions that are enzyme-dependent.

Recently, distinct evidence accumulated that ACC, as the (presumed) bioseed for bone mineral formation, is formed enzymatically *via* CA-II or CAI-IX.[17,19] The metastable ACC, readily formed under slightly alkaline conditions, undergoes rapid transformation to vaterite, and/or aragonite and calcite, unless this reaction chain is not blocked by inorganic or organic molecules.[19] In turn, in the present study we fabricated $CaCO_3$ solids, an ACC polymorph that contains a small amount of vaterite, and assessed their potential to act as (potential) bone implant material. These $CaCO_3$/polyP deposits retain the potency to undergo transformation to the stable aragonite and calcite, and additionally, after exchange of carbonate by phosphate, have the ability to form ACP and perhaps finally also HA (to be studied). Such an implant material would be superior to a biologically inert HA implant scaffold that merely functions as a mechanical place holder and platform for cells to adhere and to proliferate but not as an osteogenic material.[58]

It is established that in parallel with the enthalpy increment, crystallization of ACC to the other polymorphs (vaterite [$\approx -15$ kJ mol$^{-1}$ relative to ACC], aragonite [$\approx -19$ kJ mol$^{-1}$], or to calcite [$\approx -19$ kJ mol$^{-1}$]),[59] the solubility of ACC to vaterite, aragonite and finally calcite drops considerably between ACC and vaterite. In the present study the $Na^+$ salt of the anionic polymer polyP was added to the precursors of $CaCO_3$ ($CaCl_2$ and $Na_2CO_3$) during the synthesis of ACC. This polymer prevented, at a final concentration of 10%, the transformation process of ACC to its crystalline polymorphs vaterite, aragonite and calcite almost totally. It has been shown that the $CaCO_3$ polymorph transformation kinetics, following the Ostwald step rule, from ACC *via* the first nucleation step, the metastable spherical vaterite polymorph, then to aragonite and finally to the stable rhombohedral calcite polymorph, decreases to the same extent as the ''impurities'' in the assay increases.[60] Such an ''impurity'' is the morphogenetically active polyP that prevents the transformation from ACC to the crystalline polymorphs; only small fractions of vaterite within the ACC solid are formed.

Both the $CaCO_3$ solids[61,62] and the polyP physiological metabolite,[18,62,63] tested separately, have osteogenic potential and could serve as constituents of bioactive bone grafts. In turn, the scaffold developed in the present study exploits not only the morphogenetic potential of polyP but also utilizes the properties of this polymer to freeze the $CaCO_3$ solids at the ACC stage. This material is superior to calcite with respect to the osteogenic activity; both ''CCP5'' and ''CCP10'' are determined to be significant inducers of the gene *ALP*, a known marker for bone formation *via* stimulation of osteoblasts. This result has been obtained from studies with bone-like SaOS-2 cells and also with MSC. Using a $CaCO_3$ formulation with 10% [w/w] polyP, ''CCP10'', the release of $Ca^{2+}$, and simultaneously of $CO_3^{2-}$, is fast during the first 48 h of incubation, allowing the release of the biologically active anions $CO_3^{2-}$ and $PO_4^{3-}$ from the scaffold; the *ortho*-phosphate will be enzymatically and exohydrolytically liberated from polyP.[64] In turn, the $CO_3^{2-}$ as well as the $HCO_3^-$ anions induce the mineralization process onto bone-forming cells,[14] very likely *via* modulating the efficiency of the $HCO_3^-/Cl^-$ anion exchanger, inserted into the plasma membrane not only of osteoclasts but also of osteoblasts.[65] Very recently, this view has been corroborated by the finding that the baso-lateral anion exchanger Ae2a,b in differentiating ameloblasts secretes bicarbonates into the extracellular space under simultaneous deposition of HA/enamel.[66]

To assess the biocompatibility of the $CaCO_3$/polyP material *in vivo*, ''CCP10'' was encapsulated into PLGA (''polyP-mic'') microspheres. In parallel, the control implant spheres remained without $CaCO_3$/polyP (''cont-mic''). Those pearls were inserted into the muscles of the back of rats. After an observation period of 2, 4, and 8 weeks tissue samples were taken from the rats and inspected microscopically after slicing and staining with Mayer's hematoxylin. The inspections show that in the ''polyP-mic'' series an advanced repopulation of the implant region with cells became evident after 4 weeks and 8 weeks, resp. In contrast, the microspheres lacking $CaCO_3$/polyP were devoid of any cells. From these experiments we conclude that the ''CCP10'' biomaterial is not only biocompatible but also supports the cellular regeneration potency of the impaired implant region.

## 5. Conclusion

The recently gathered findings on the $CaCO_3$ nature of the bioseeds, the anion exchange of $CO_3^{2-}$ by $PO_4^{3-}$ and the supply of *ortho*-phosphate from polyP, the following series of mechanistically distinct processes, describing bone formation, can be sketched. In the first phase during bone mineral deposition, like in the endochondral ossification, the cartilage in the metaphysis comprising the growth center between the epiphysis and the diaphysis of the long bone, calcifies. It is likely that this process of calcification is enzymatically driven by CA-II and/or CA-IX. Secondly, platelets which accumulate with the osteoblasts both in regions of bone formation and also at bone fracture sites release polyP into the extracellular space where the polymer undergoes ALP-mediated exohydrolysis under the release of *ortho*-phosphate. Thirdly, the available phosphate units, formed in a spatial vicinity to the bioseed synthesis,

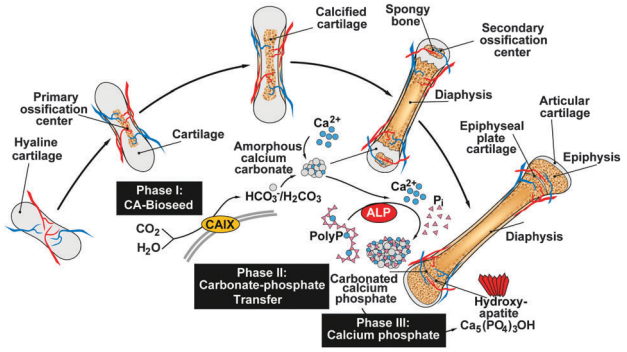


Fig. 11 Schematic presentation of the process of endochondral ossification and the proposed phases of bone mineral deposition. After penetration of blood vessels the hyaline cartilage at the primary ossification centers in the diaphysis starts to calcify ($CaCO_3$ deposits). The formation of spongy bone at the secondary ossification centers in the epiphyses starts later. Two regions of hyaline cartilage remain the articular cartilage at the surface of the epiphysis and the epiphyseal plate (growth region) between the epiphysis and diaphysis. The mineral deposition in the growth region is subdivided into the following three steps. Phase I: amorphous calcium carbonate (ACC) bioseeds are formed, a process which might be mediated by the membrane-associated CA-IX. Phase II: polyP released from platelets undergoes ALP-mediated hydrolysis under the formation of *ortho*-phosphate that acts as a phosphate donor for the carbonate-phosphate transfer reaction. Finally phase III: the phosphate units are used for (carbonated) calcium phosphate formation.

serve as the source for the formation of ACP and ultimately to carbonated HA; Fig. 11.

Considering this background, the $CaCO_3$/polyP material fabricated in this paper appears to be a promising biocompatible and osteogenic scaffold that provides both the substrate for the bioseed development ($CaCO_3$ [$CO_3^{2-}$]) and for the subsequent transformation to the calcium phosphate (polyP [$PO_4^{3-}$]).

## Acknowledgements

W.E.G. M. is a holder of an ERC Advanced Investigator Grant. We thank Dipl. Ing. G. Glaßer (“Elektronenmikroskopie”; Max Planck Institute for Polymer Research, Mainz, Germany) for very expert and helpful SEM analyses. Furthermore we are grateful to Dr V. Mailänder (Max Planck Institute for Polymer Research, Mainz, Germany) for gifting mesenchymal stem cells. This work was supported by grants from the European Commission (ERC Advanced Investigator Grant “BIOSILICA”: No. 268476; “Bio-Scaffolds”: No. 604036 and “BlueGenics”: No. 311848), the Deutsche Forschungsgemeinschaft (Schr 277/10-3), and the International Human Frontier Science Program.

## Notes and references

1 O. Braissant, G. Cailleau, C. Dupraz and E. P. Verrecchia, Bacterially induced mineralization of calcium carbonate in terrestrial environments: the role of exopolysaccharides and amino acids, *J. Sediment. Res.*, 2003, **73**, 485–490.
2 F. C. Meldrum and H. Cölfen, Controlling mineral morphologies and structures in biological and synthetic systems, *Chem. Rev.*, 2008, **108**, 4332–4432.
3 F. C. Meldrum, Calcium carbonate in biomineralisation and biomimetic chemistry, *Int. Mater. Rev.*, 2003, **48**, 187–224.
4 D. Ren, Q. Feng and X. Bourrat, Effects of additives and templates on calcium carbonate mineralization *in vitro*, *Micron*, 2011, **42**, 228–245.
5 J. Tomás, A. J. Geffen, I. S. Allen and J. Berges, Analysis of the soluble matrix of vaterite otoliths of juvenile herring (*Clupea harengus*): do crystalline otoliths have less protein?, *Comp. Biochem. Physiol., Part A: Mol. Integr. Physiol.*, 2004, **139**, 301–308.
6 A. M. Oliveira, M. Farina, I. P. Ludka and B. Kachar, Vaterite, calcite, and aragonite in the otoliths of three species of *Piranha*, *Naturwissenschaften*, 1996, **83**, 133–135.
7 G. Falini, S. Albeck, S. Weiner and L. Addadi, Control of aragonite or calcite polymorphism by mollusk shell macromolecules, *Science*, 1996, **271**, 67–69.
8 W. E. G. Müller, M. Neufurth, U. Schlossmacher, H. C. Schröder, D. Pisignano and X. H. Wang, The sponge silicatein-interacting protein silintaphin-2 blocks calcite formation of calcareous sponge spicules at the vaterite stage, *RSC Adv.*, 2014, **4**, 2577–2585.
9 L. Addadi and S. Weiner, Interactions between acidic proteins and crystals: stereochemical requirements in biomineralization, *Proc. Natl. Acad. Sci. U. S. A.*, 1985, **82**, 4110–4114.
10 X. Liu, S. Zeng, S. Dong, C. Jin and J. Li, A novel matrix protein hic31 from the prismatic layer of *Hyriopsis cumingii* displays a collagen-like structure, *PLoS One*, 2015, **10**(8), e0135123.
11 S. Weiner and H. D. Wagner, The material bone: structure-mechanical function relations, *Annu. Rev. Mater. Res.*, 1998, **28**, 271–298.
12 N. Reznikov, R. Shahar and S. Weiner, Bone hierarchical structure in three dimensions, *Acta Biomater.*, 2014, **10**, 3815–3826.
13 Y. Wang, S. Von Euw, F. M. Fernandes, S. Cassaignon, M. Selmane, G. Laurent, G. Pehau-Arnaudet, C. Coelho, L. Bonhomme-Coury, M. M. Giraud-Guille, F. Babonneau, T. Azaïs and N. Nassif, Water-mediated structuring of bone apatite, *Nat. Mater.*, 2013, **12**, 1144–1153.
14 X. H. Wang, H. C. Schröder, U. Schlossmacher, M. Neufurth, Q. Feng, B. Diehl-Seifert and W. E. G. Müller, Modulation of the initial mineralization process of SaOS-2 cells by carbonic anhydrase activators and polyphosphate, *Calcif. Tissue Int.*, 2014, **94**, 495–509.
15 S. Y. Liao, M. I. Lerman and E. J. Stanbridge, Expression of transmembrane carbonic anhydrases, CAIX and CAXII, in human development, *BMC Dev. Biol.*, 2009, **9**, 22, DOI: 10.1186/1471-213X-9-22.
16 X. Chang, Y. Zheng, Q. Yang, L. Wang, J. Pan, Y. Xia, X. Yan and J. Han, Carbonic anhydrase I (CA1) is involved in the process of bone formation and is susceptible to ankylosing spondylitis, *Arthritis Res.*, 2012, **14**, R176.
17 W. E. G. Müller, H. C. Schröder, E. Tolba, M. Neufurth, B. Diehl-Seifert and X. H. Wang, Mineralization of bone-related SaOS-2 cells under physiological hypoxic conditions, *FEBS J.*, 2015, in press.

 

18 X. H. Wang, H. C. Schröder and W. E. G. Müller, Polyphosphate as a metabolic fuel in Metazoa: A foundational breakthrough invention for biomedical applications, *Biotechnol. J.*, 2015, DOI: 10.1002/biot.201500168.

19 W. E. G. Müller, M. Neufurth, J. Huang, K. Wang, Q. Feng, H. C. Schröder, B. Diehl-Seifert, R. Muñoz-Espí and X. H. Wang, Non-enzymatic transformation of amorphous $CaCO_3$ into calcium phosphate mineral after exposure to sodium phosphate *in vitro*: Implications for *in vivo* hydroxyapatite bone formation, *ChemBioChem*, 2015, **16**, 1323–1332.

20 S. Omelon, J. Georgiou, F. Variola and M. N. Dean, Colocation and role of polyphosphates and alkaline phosphatase in apatite biomineralization of elasmobranch tesserae, *Acta Biomater.*, 2014, **10**, 3899–3910.

21 W. E. Brown, J. P. Smith, J. R. Lehr and A. W. Frazier, Crystallographic and chemical relations between octacalcium phosphate and hydroxyapatite, *Nature*, 1962, **196**, 1050–1055.

22 S. Bose, M. Roy and A. Bandyopadhyay, Recent advances in bone tissue engineering scaffolds, *Trends Biotechnol.*, 2012, **30**, 546–554.

23 R. Guzmán, S. Nardecchia, M. C. Gutiérrez, M. L. Ferrer, V. Ramos, F. del Monte, A. Abarrategi and J. L. López-Lacomba, Chitosan scaffolds containing calcium phosphate salts and rhBMP-2: *in vitro* and *in vivo* testing for bone tissue regeneration, *PLoS One*, 2014, **9**(2), e87149.

24 M. Kellermeier, E. Melero-García, F. Glaab, R. Klein, M. Drechsler, R. Rachel, J. M. García-Ruiz and W. Kunz, Stabilization of amorphous calcium carbonate in inorganic silica-rich environments, *J. Am. Chem. Soc.*, 2010, **132**, 17859–17866.

25 K. Sawada, The mechanisms of crystallization and transformation of calcium carbonates, *Pure Appl. Chem.*, 1997, **69**, 921–928.

26 J. Ihli, A. N. Kulak and F. C. Meldrum, Freeze-drying yields stable and pure amorphous calcium carbonate (ACC), *Chem. Commun.*, 2013, **49**, 3134–3136.

27 R. Schröder, H. Pohlit, T. Schüler, M. Panthöfer, R. E. Unger, H. Frey and W. Tremel, Transformation of vaterite nanoparticles to hydroxycarbonate apatite in a hydrogel scaffold: Relevance to bone formation, *J. Mater. Chem. B*, 2015, **3**, 7079–7089.

28 W. E. G. Müller, E. Tolba, H. C. Schröder, S. Wang, G. Glaßer, R. Muñoz-Espí, T. Link and X. H. Wang, A new polyphosphate calcium material with morphogenetic activity, *Mater. Lett.*, 2015, **148**, 163–166.

29 W. E. G. Müller, E. Tolba, H. C. Schröder, B. Diehl-Seifert and X. H. Wang, Retinol encapsulated into amorphous $Ca^{2+}$ polyphosphate nanospheres acts synergistically in MC3T3-E1 cells, *Eur. J. Pharm. Biopharm.*, 2015, **93**, 214–223.

30 R. M. Pilliar, M. J. Filiaggi, J. D. Wells, M. D. Grynpas and R. A. Kandel, Porous calcium polyphosphate scaffolds for bone substitute applications – *in vitro* characterization, *Biomaterials*, 2001, **22**, 963–972.

31 Y. Shanjani, J. N. De Croos, R. M. Pilliar, R. A. Kandel and E. Toyserkani, Solid freeform fabrication and characterization of porous calcium polyphosphate structures for tissue engineering purposes, *J. Biomed. Mater. Res., Part B*, 2010, **93**, 510–519.

32 B. Lee, M. Kim, S. Choi and Y. K. Lee, Amorphous calcium polyphosphate bone regenerative materials based on calcium phosphate glass, *Key Eng. Mater.*, 2009, **396–398**, 209–212.

33 J. H. Morrissey, S. H. Choi and S. A. Smith, Polyphosphate: an ancient molecule that links platelets, coagulation, and inflammation, *Blood*, 2012, **119**, 5972–5979.

34 L. Faxälv, N. Boknäs, J. O. Ström, P. Tengvall, E. Theodorsson, S. Ramström and T. L. Lindahl, Putting polyphosphates to the test: evidence against platelet-induced activation of factor XII, *Blood*, 2013, **122**, 3818–3824.

35 S. Raynaud, E. Champion, D. Bernache-Assollant and P. Thomas, Calcium phosphate apatites with variable Ca/P atomic ratio I. Synthesis, characterisation and thermal stability of powders, *Biomaterials*, 2002, **23**, 1065–1072.

36 K. Saito, H. Omori, S. Kanno, Y. Hirata, T. Okada, S. Mori and K. Nakadate, Chemical and crystallographic studies on 33 cases of calcium carbonate gallstone (so-called limy bile), *Gastroenterol. Jpn.*, 1986, **21**, 162–166.

37 Q. Hu, J. Zhang, H. Teng and U. Becker, Growth process and crystallographic properties of ammonia-induced vaterite, *Am. Mineral.*, 2012, **97**, 1437–1445.

38 U. Schloßmacher, H. C. Schröder, X. H. Wang, Q. Feng, B. Diehl-Seifert, S. Neumann, A. Trautwein and W. E. G. Müller, Alginate/silica composite hydrogel as a potential morphogenetically active scaffold for three-dimensional tissue engineering, *RSC Adv.*, 2013, **3**, 11185–11194.

39 M. Wiens, X. Wang, H. C. Schröder, U. Kolb, U. Schlossmacher, H. Ushijima and W. E. G. Müller, The role of biosilica in the osteoprotegerin/RANKL ratio in human osteoblast-like cells, *Biomaterials*, 2010, **31**, 7716–7725.

40 M. Wiens, X. Wang, U. Schlossmacher, I. Lieberwirth, G. Glasser, H. Ushijima, H. C. Schröder and W. E. G. Müller, Osteogenic potential of biosilica on human osteoblast-like (SaOS-2) cells, *Calcif. Tissue Int.*, 2010, **87**, 513–524.

41 M. R. Lorenz, V. Holzapfel, A. Musyanovych, K. Nothelfer, P. Walther, H. Frank, K. Landfester, H. Schrezenmeier and V. Mailänder, Uptake of functionalized, fluorescent-labeled polymeric particles in different cell lines and stem cells, *Biomaterials*, 2006, **27**, 2820–2828.

42 X. H. Wang, H. C. Schröder, V. Grebenjuk, B. Diehl-Seifert, V. Mailänder, R. Steffen, U. Schloßmacher and W. E. G. Müller, The marine sponge-derived inorganic polymers, biosilica and polyphosphate, as morphogenetically active matrices/scaffolds for differentiation of human multipotent stromal cells: Potential application in 3D printing and distraction osteogenesis, *Mar. Drugs*, 2014, **12**, 1131–1147.

43 H. C. Schröder, X. H. Wang, M. Wiens, B. Diehl-Seifert, K. Kropf, U. Schloßmacher and W. E. G. Müller, Silicate modulates the cross-talk between osteoblasts (SaOS-2) and osteoclasts (RAW 264.7 cells): inhibition of osteoclast growth and differentiation, *J. Cell. Biochem.*, 2012, **113**, 3197–3206.

44 S. F. Wang, X. H. Wang, F. G. Draenert, O. Albert, H. C. Schröder, V. Mailänder, G. Mitov and W. E. G. Müller, Bioactive and biodegradable silica biomaterial for bone regeneration, *Bone*, 2014, **67**, 292–304.

45 M. S. Mahadevaiah, Y. Kumar, M. S. Abdul-Galil, M. S. Suresha, M. A. Sathish and G. Nagendrappa, A simple spectrophotometric determination of phosphate in sugarcane juices, water and detergent samples, *E-J. Chem.*, 2007, **4**, 467–473.

46 D. Chavan, T. C. van de Watering, G. Gruca, J. H. Rector, K. Heeck, M. Slaman and D. Iannuzzi, Ferrule-top nanoindenter: an optomechanical fiber sensor for nanoindentation, *Rev. Sci. Instrum.*, 2012, **83**, 115110, DOI: 10.1063/1.4766959.

47 S. Vidya, A. Parameswaran and V. G. Sugumaran, Comparative evaluation of tissue. Compatibility of three root canal. Sealants in Rattus norwegicus: A Histopathological study, *Endodontology*, 1994, **6**, 7–17.

48 J. M. Anderson, Biological responses to materials, *Annu. Rev. Mater. Res.*, 2001, **31**, 81–110.

49 H. R. Lee, H. J. Kim, J. S. Ko, Y. S. Choi, M. W. Ahn, S. Kim and S. H. Do, Comparative characteristics of porous bioceramics for an osteogenic response *in vitro* and *in vivo*, *PLoS One*, 2013, **8**, e84272.

50 L. Sachs, *Angewandte Statistik*, Springer, Berlin, 1984, p. 242.

51 I. W. Kim, J. L. Giocondi, C. Orme, S. Collino and J. S. Evans, Morphological and kinetic transformation of calcite crystal growth by prismatic-associated asprich sequences, *Cryst. Growth Des.*, 2008, **8**, 1154–1160.

52 C. Pautke, M. Schieker, T. Tischer, A. Kolk, P. Neth, W. Mutschler and S. Milz, Characterization of osteosarcoma cell lines MG-63, Saos-2 and U-2 OS in comparison to human osteoblasts, *Anticancer Res.*, 2004, **24**, 3743–3748.

53 A. Oyane, H. M. Kim, T. Furuya, T. Kokubo, T. Miyazaki and T. Nakamura, Preparation and assessment of revised simulated body fluids, *J. Biomed. Mater. Res., Part A*, 2003, **65**, 188–195.

54 B. Clarke, Normal bone anatomy and physiology, *Clin. J. Am. Soc. Nephrol.*, 2008, **3**(suppl 3), S131–S139.

55 M. R. Wiederkehr and O. W. Moe, Uric acid nephrolithiasis: A systemic metabolic disorder, *Clin. Rev. Bone Miner. Metab.*, 2011, **9**, 207–217.

56 M. N. Rahaman, D. E. Day, B. S. Bal, Q. Fu, S. B. Jung, L. F. Bonewald and A. P. Tomsia, Bioactive glass in tissue engineering, *Acta Biomater.*, 2011, **7**, 2355–2373.

57 J. D. Termine and A. S. Posner, Amorphous/crystalline interrelationships in bone mineral, *Calcif. Tissue Res.*, 1967, **1**, 8–23.

58 H. Wang, Y. Li, Y. Zuo, J. Li, S. Ma and L. Cheng, Biocompatibility and osteogenesis of biomimetic nano-hydroxyapatite/polyamide composite scaffolds for bone tissue engineering, *Biomaterials*, 2007, **28**, 3338–3348.

59 A. V. Radha, T. Z. Forbes, C. E. Killian, P. U. Gilbert and A. Navrotsky, Transformation and crystallization energetics of synthetic and biogenic amorphous calcium carbonate, *Proc. Natl. Acad. Sci. U. S. A.*, 2010, **107**, 16438–16443.

60 A. Richter, D. Petzold, H. Hofmann and B. Ullrich, Production, properties and application of calcium carbonate powders. 3. Investigations to the transition of vaterite and aragonite in aqueous systems, *Chem. Tech.*, 1996, **48**, 271–275.

61 K. Kuroda, M. Moriyama, R. Ichino, M. Okido and A. Seki, Formation and *in vivo* evaluation of carbonate apatite and carbonate apatite/$CaCO_3$ composite films using the thermal substrate method in aqueous solution, *Mater. Trans.*, 2008, **49**, 1434–1440.

62 X. H. Wang, H. C. Schröder and W. E. G. Müller, Enzyme-based biosilica and biocalcite: biomaterials for the future in regenerative medicine, *Trends Biotechnol.*, 2014, **32**, 441–447.

63 W. E. G. Müller, E. Tolba, H. C. Schröder, M. Neufurth, S. Wang, T. Link, B. Al-Nawas and X. H. Wang, A new printable and durable *N*,*O*-carboxymethyl chitosan–$Ca^{2+}$–polyphosphate complex with morphogenetic activity, *J. Mater. Chem. B*, 2015, **3**, 1722–1730.

64 W. E. G. Müller, X. H. Wang, B. Diehl-Seifert, K. Kropf, U. Schloßmacher, I. Lieberwirth, G. Glasser, M. Wiens and H. C. Schröder, Inorganic polymeric phosphate/polyphosphate as an inducer of alkaline phosphatase and a modulator of intracellular $Ca^{2+}$ level in osteoblasts (SaOS-2 cells) *in vitro*, *Acta Biomater.*, 2011, **7**, 2661–2671.

65 J. Green, D. T. Yamaguchi, C. R. Kleeman and S. Muallem, Cytosolic pH regulation in osteoblasts. Regulation of anion exchange by intracellular pH and $Ca^{2+}$ ions, *J. Gen. Physiol.*, 1990, **95**, 121–145.

66 R. Jalali, B. Zandieh-Doulabi, P. K. DenBesten, U. Seidler, B. Riederer, S. Wedenoja, D. Micha and A. L. Bronckers, Slc26a3/Dra and Slc26a6 in murine ameloblasts, *J. Dent. Res.*, 2015, DOI: 10.1177/0022034515606873.

 